Intrinsic and impurity-induced emission bands in $SrHfO_3$

E. Mihóková,[1,2] N. Chiodini,[1] M. Fasoli,[1] A. Lauria,[1] F. Moretti,[1] M. Nikl,[2] V. Jarý,[2] and A Vedda[1]
[1]*Dip. di Scienza dei Materiali, Università di Milano-Bicocca, via Cozzi 53, 20125 Milano, Italy*
[2]*Institute of Physics, Academy of Sciences of the Czech Republic, v.v.i., Cukrovarnická 10, 16253 Prague, Czech Republic*
(Received 3 July 2010; revised manuscript received 14 September 2010; published 15 October 2010)

To better understand the scintillation mechanism in $SrHfO_3$-based scintillators we investigate in detail their x-ray excited radioluminescence (RL) emissions. The Gaussian decomposition of the undoped $SrHfO_3$ RL spectra manifests the presence of four emission bands peaking at 3.0, 4.0, 4.6, and 5.1 eV. Based on corresponding photoluminescence emission and excitation spectra we tentatively associate the observed bands with excitonic or defect-related emissions. When doped by Ce^{3+} or Pb^{2+} luminescent activators, the RL spectra feature two or three new bands, respectively. The temperature dependence of all RL spectra demonstrates a competition between activators and intrinsic or defect centers in carrier capture. Around room temperature the emission process is completely dominated by recombination at activator centers. In the case of Pb^{2+} activator we also study in detail the concentration dependence of the RL spectra below room temperature exhibiting an optimal value around 0.3 mol %.

DOI: 10.1103/PhysRevB.82.165115 PACS number(s): 78.70.Ps

I. INTRODUCTION

$SrHfO_3$ as well as other alkaline-earth hafnates has been studied from 1930s. The research interest was focused on its application in microelectronics (high k materials),[1] microwave ceramics resonators,[2] or thermal barrier coatings.[3] Due to its high density (7.56 g/cm^3) and high effective atomic number it also became potentially interesting as a scintillator host. Blue emitting phosphor $SrHfO_3:Tm^{3+}$ is reported in Ref. 4. $SrHfO_3:Ce^{3+}$, discovered as an efficient phosphor,[5] is currently rather vividly investigated. Compared to $Bi_4Ge_3O_{12}$ it has twice higher light output and is five times faster. Because of its high melting point ($T_m > 2400$ °C) it is not available as a single crystal. Possible alternatives include transparent ceramics or nanocrystals embedded in an inert host. The scintillation properties of Ce-doped $SrHfO_3$ and $BaHfO_3$ ceramics obtained from powders prepared by solid-state synthesis were studied in Ref. 6 while nanocrystals of $SrHfO_3$ prepared by combustion synthesis were reported in Refs. 7 and 8. The preparation of Ce-doped $SrHfO_3$ powders via sol-gel route is presented in Refs. 9 and 10.

Recently we reported optical and structural characteristics of $SrHfO_3$ powder samples prepared by acetate and citrate combustion[11] and solid-state reaction.[12] In addition to Ce-doped $SrHfO_3$ we also introduced a different potentially interesting scintillator, Pb-doped $SrHfO_3$. The radioluminescence (RL) at room temperature (RT) strongly depended on the final sintering temperature. $SrHfO_3:Pb^{2+}$ has the RL efficiency slightly higher than that of $SrHfO_3:Ce^{3+}$. Its photoluminescence (PL) decay was thoroughly studied in Ref. 12 showing a decay time of about 190 ns at RT while that of $SrHfO_3:Ce^{3+}$ was 15 ns. The RT dependence of RL on the concentration of activator ions together with the evolution of the structural and morphological properties during the powder sintering was studied in Ref. 13. The results reported in Ref. 14 evidence a thermally induced ionization of the Ce^{3+} excited state in the $SrHfO_3$ host, an undesired phenomenon deteriorating the scintillation performance of the material.

All previous above-mentioned studies of $SrHfO_3$ are application oriented, addressing preparation techniques and basic optical and scintillation characteristics. However, the knowledge of energy transfer and localization processes in the host matrix is crucial for optimizing scintillator performance once a suitable activator is incorporated. Given the activator-excited-state thermally induced ionization,[14] its role becomes yet more relevant. That is why the present work is focused on understanding the underlying scintillation mechanisms in the $SrHfO_3$ host. We investigate in detail the x-ray excited RL emissions in the $SrHfO_3$-based scintillators. We analyze RL emission spectra of undoped $SrHfO_3$ together with corresponding PL emission and excitation spectra and tentatively associate the observed bands with excitonic or defect related emissions. The similar analysis performed for $SrHfO_3$ doped by Ce^{3+} or Pb^{2+} luminescent activators demonstrates the competition between activators and intrinsic or defect centers in carrier capture. We also study in detail the concentration dependence of the $SrHfO_3:Pb^{2+}$ RL emissions.

II. EXPERIMENTAL DETAILS

A. Samples and experimental techniques

Undoped as well as Ce^{3+}- and Pb^{2+}-doped $SrHfO_3$ samples were prepared by acetate and citrate combustion (A-C combustion) at the Department of Materials Science of the University of Milano-Bicocca, Milano (Italy). The preparation technique is described elsewhere.[11,13] Dopant concentrations were 0.1 mol % for Ce^{3+} and 0.03, 0.1, 0.3, 1.0, and 3.0 mol % for Pb^{2+}. Final sintering temperature was 1150 °C. $SrHfO_3:Pb^{2+}$ with an intermediate concentration of 0.3 mol % was also prepared by solid-state reaction in the Institute of Physics, ASCR, Prague (Czech Republic).[12] In this case the final sintering temperature was 1200 °C.

X-ray excited RL measurements were performed with a homemade apparatus featuring a charge coupled device detector (Jobin-Yvon Spectrum One 3000) coupled to a monochromator (Jobin-Yvon Triax 180) with 100 grooves/mm grating operating in the 200–1100 nm interval. X-ray irradiations were performed by a Philips 2274 tube operated at 20

kV. PL excitation and emission spectra excited by a H_2 steady-state lamp were measured by a custom made 5000M Horiba Jobin Yvon spectrofluorometer. Steady-state excitation spectra in the UV-vacuum ultraviolet region were measured at the Superlumi station in DESY laboratories (Hamburg, Germany). All spectra are corrected for the instrumental responses of the apparatuses.

B. Numerical analysis

All measured RL spectra have been decomposed to a sum of several Gaussians. The number of free parameters is high and therefore the fitting procedure had to be carefully performed to avoid unphysical or ambiguous solutions of the minimization algorithm. Taking this into account we performed the decomposition in the following way. We started the decomposition of the spectrum measured at the lowest temperature where the maximum number of elementary bands is present. We only considered bands that are clearly recognizable in the measured spectrum using the naked eye. The resulting (and satisfactory) fit provided the Gaussian parameters of the bands. We kept the positions and widths of the bands within a narrow range and proceeded toward decompositions at higher temperatures where the same bands had to be recognized, only allowing their intensity to change. With consistent spectral positions and widths we succeeded in fitting the whole set of the spectra measured in a wide temperature range.

III. RESULTS AND DISCUSSION

A. $SrHfO_3$ undoped

In Fig. 1(a) we present x-ray excited RL spectra of undoped $SrHfO_3$ in the temperature interval 10–310 K. The RL intensity monotonically decreases with increasing temperature. We note that the tip around 3.3 eV is due to an experimental artifact caused by the spectral correction of the data. The Gaussian decomposition of all spectra shows the presence of four bands at 3.0, 4.0, 4.6, and 5.1 eV as demonstrates an example reported in Fig. 1(b) corresponding to the measurement performed at 10 K. The band at 3.4 eV is added to satisfactorily fit the data containing the experimental artifact mentioned above (the parameters of all Gaussians are listed in Table I). The temperature evolution of the relative intensity of each peak with respect to the total emission intensity is shown in Fig. 1(c).

The high energy bands at 4.6 and 5.1 eV manifest a similar temperature evolution. The low-temperature slight increase up to about 50 K turns to a rapid decrease and at about 150 K both bands completely vanish [cf. Fig. 1(c)]. Their vicinity to the band edge (about 6.1 eV) as well as their temperature evolution suggests their association with two excitonic states. The excitation spectrum of the highest energy 5.1 eV band is displayed in Fig. 2. Ce-doped $SrHfO_3$ is also shown for comparison. As the excitation of the Ce^{3+} emission at energies above the gap most probably occurs due to the consecutive capture of an electron and a hole, the edge between 5.9 and 6.2 eV can indicate the band-to-band transition onset. Therefore the excitation peak of the undoped

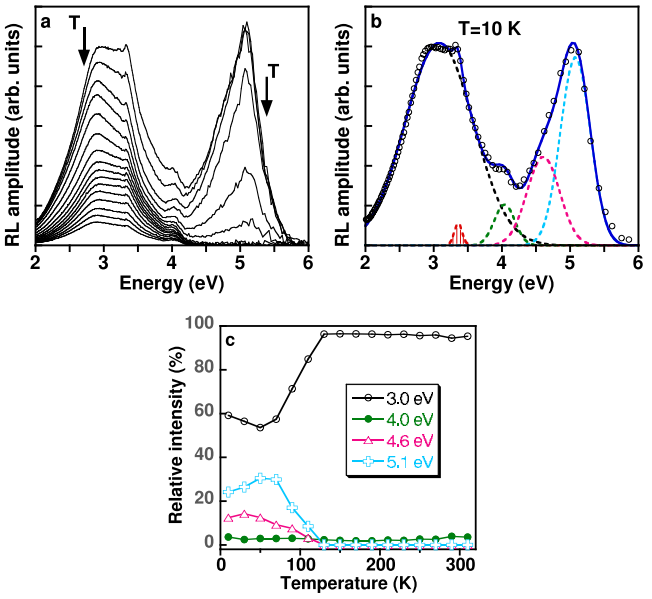

FIG. 1. (Color online) (a) X-ray excited RL spectra of undoped $SrHfO_3$ in the 10–310 K temperature interval, the arrows indicate the evolution of the spectra with increasing temperature. (b) Example of the Gaussian decomposition of the RL spectrum at 10 K. Empty circles are experimental data, solid line is the fit of the sum of five Gaussians to the data, and dashed lines are Gaussian components. Hatched Gaussian at 3.4 eV is an artificial band added due to experimental artifact (see the text). (c) Temperature evolution of relative intensity of each peak with respect to the total emission intensity; the spectral position of each peak is indicated in the legend.

sample slightly below the edge at around 6 eV could correspond to the exciton absorption peak. This peak measured at 10 K and 4.8 eV (Fig. 3) is apparently high-energy shifted with respect to the spectrum in Fig. 2, which is an expected temperature evolution of the exciton absorption. The large Stokes shift (0.9 eV) and the broadness of the band suggest that the 5.1 eV RL band would be the emission of the self-trapped exciton (STE). Excitation spectrum of the 4.6 eV band was measured at 77 K and the emission energy 4.5 eV to exclude a contribution of the 5.1 eV emission. The ascending part of the excitation spectrum of exciton emission above 5.9 eV (cf. Fig. 3)[15] confirms that the 4.6 eV band is also excited in the exciton absorption region suggesting its excitonic origin. Even though the presence of the weak excitation band at about 5.4 eV does not entirely exclude a defect contribution, it most likely corresponds to the slight participation of the 4.0 eV band in the emission at 4.5 eV. The excitonic character of the 4.6 eV band is mostly favored by the similar temperature evolution as that of the 5.1 eV band. Emission spectrum excited at 6.2 eV and 77 K (Fig. 3) shows the presence of 5.1 eV as well as an indication of 4.6 eV bands and the emission band at 2.7 eV (discussed later).

To summarize all the above, the 5.1 eV band can be associated with STE and the 4.6 eV band can either be the second emission state of STE or an exciton trapped around impurity or lattice defect. Its association with the second state of the STE would be plausible provided the population of two different emitting states is set in the unrelaxed STE

TABLE I. Mean parameter values of the Gaussian components obtained by the RL spectra decomposition in the temperature interval 10–310 K. For the band origin designation, see the text.

Band origin	(eV)	$SrHfO_3$	$SrHfO_3:Pb^{2+}$	$SrHfO_3:Ce^{3+}$
$TE_{II}+DE_I$	Center	3.02 ± 0.03	3.28 ± 0.04	3.21 ± 0.09
	FWHM	1.09 ± 0.04	1.44 ± 0.08	1.30 ± 0.10
Activator	Center		3.60 ± 0.01	3.04 ± 0.01
	FWHM		0.50 ± 0.20	0.38 ± 0.03
Activator	Center		3.74 ± 0.02	3.31 ± 0.01
	FWHM		0.41 ± 0.06	0.26 ± 0.02
Pb^{2+} contamination	Center			3.50 ± 0.10
	FWHM			0.14 ± 0.03
DE_{II}	Center	4.03 ± 0.01	4.03 ± 0.01	4.14 ± 0.05
	FWHM	0.28 ± 0.05	0.02 ± 0.02	0.31 ± 0.05
Activator-perturbed TE_I	Center		4.35 ± 0.04	4.32 ± 0.05
	FWHM		0.69 ± 0.03	0.83 ± 0.04
TE_I	Center	4.60 ± 0.02		4.59 ± 0.02
	FWHM	0.55 ± 0.04		0.60 ± 0.20
STE	Center	5.09 ± 0.01	5.03 ± 0.01	5.11 ± 0.03
	FWHM	0.52 ± 0.02	0.61 ± 0.08	0.50 ± 0.10

excited state with no further exchange between the two relaxed excited states. Such energy exchange would induce a temperature evolution of two STE bands being substantially different rather than similar as observed [cf. Fig. 1(c)]. On the other hand, the deeper state corresponding to the 4.6 eV band would become initially more populated and consequently more intense comparing to the shallower state corresponding to the 5.1 eV band, hence being in contrast to what we observe [cf. Fig. 1(c)]. Accordingly, we associate the 4.6 eV band with the trapped exciton that we designate TE_I. Simultaneous disappearance of both exciton bands (5.1 and 4.6 eV) at about 150 K might be due to a thermal disintegration of both excitons having a similar binding energy.

The recombination center responsible for the low energy RL band at 3.0 eV is the most efficient in the material. The 3.0 eV band seems analogous to the visible green (2.4 eV) or blue-violet (2.9 eV) photoluminescence bands observed in $SrTiO_3$ (or $PbTiO_3$) and $SrZrO_3$, respectively, see, e.g.,[16–19]

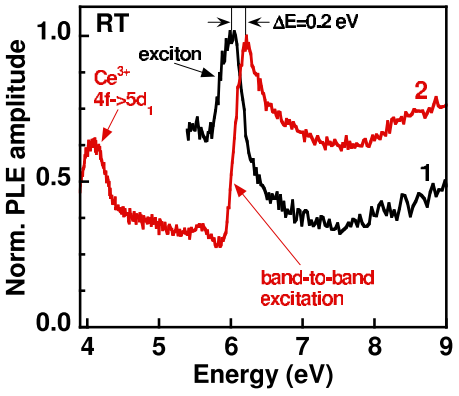

FIG. 2. (Color online) Normalized PL excitation spectra at RT. In curve 1, undoped $SrHfO_3$, $E_{em}=5.2$ eV. In curve 2, SrHfO3:Ce (0.1 mol %) with $E_{em}=3.2$ eV is shown for comparison.

Considering that $SrZrO_3$ has similar structure (orthorhombic) as well as similar band gap [5.6 eV (Ref. 20)] comparing to $SrHfO_3$ one would expect an analogous band in $SrHfO_3$ appearing at a similar energy, which is actually the case. There is an extensive literature devoted to interpretation of these bands. The most recent[16] based on both theoretical and experimental data attributed the visible bands in $SrTiO_3$ and $SrZrO_3$ to lattice disorder. Experimentally, the bands were observed in quasicrystalline powders. As the order of the lattice increased the emission bands disappeared. Due to the high crystallinity of our powders as shown by x-ray-diffraction data[11] this interpretation does not seem applicable. According to others, the green emission in $SrTiO_3$ is intrinsic, corresponding to the recombination of STEs,[17] or new polaronic-type excitons, charge-transfer vibronic excitons,[18] a concept introduced to explain an exciton structure in ABO_3-type materials.[21–23] The latter conclusions were

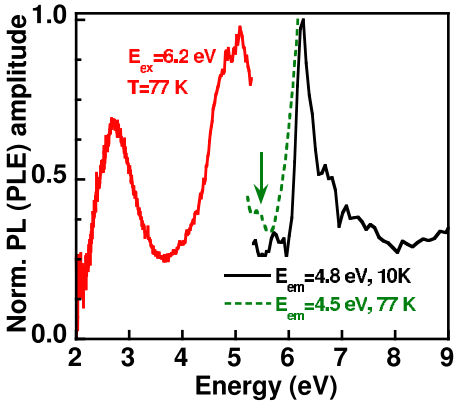

FIG. 3. (Color online) Normalized PL excitation spectra of $SrHfO_3$ at 4.8 eV, 10 K as well as at 4.5 eV, 77 K and PL emission spectrum at 6.2 eV, 77 K. The arrow indicates the presence of the weak excitation band at about 5.4 eV.

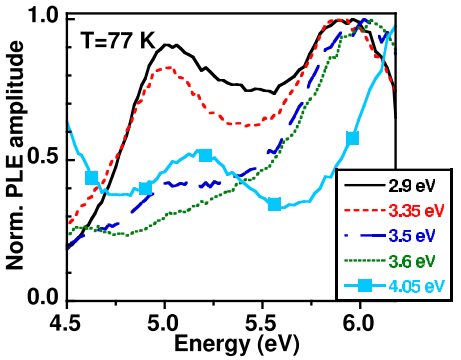

FIG. 4. (Color online) Normalized PL excitation spectra of $SrHfO_3$ at 77 K. Emission energies are reported in the legend.

based on experimental data partly obtained for single-crystal samples, therefore materials of high degree of crystallinity as in our samples.

To better understand the nature of the 3.0 eV RL band in undoped $SrHfO_3$ we studied corresponding PL excitation and emission spectra. Photoluminescence excitation spectra measured around the maximum of the RL band at 2.9 eV exhibit two excitation peaks at about 5.0 and 5.9 eV (see Fig. 4). The high-energy peak well matches the exciton absorption peak (6.0 eV) discussed above. Its low-energy shift is due to mixing with the 5.0 eV band. The low-energy excitation band is probably connected to excitation of some impurity or lattice defect. When PL emission is excited at 5.93 eV and 5.06 eV, the emission band shifts from 2.8 eV to 3.0 eV, respectively (cf. Fig. 5). Such shift implies that the PL and consequently also RL bands around 3.0 eV actually have a composed character. The affirmation is confirmed by the Gaussian decomposition of the PL emission band observed under both excitations, either within defect (5.03 eV) or exciton absorption (5.93 eV) displayed in Figs. 6(a) and 6(b). In both cases the PL band is composed of two Gaussians G_1 and G_2 centered at about 2.7 ± 0.1 eV and 3.1 ± 0.1 eV, respectively.[24] The excitation spectra measured at progressively increasing emission energy from 2.9 to 3.6 eV exhibit a gradual intensity reduction of the 5.0 eV excitation band (see Fig. 4). We note

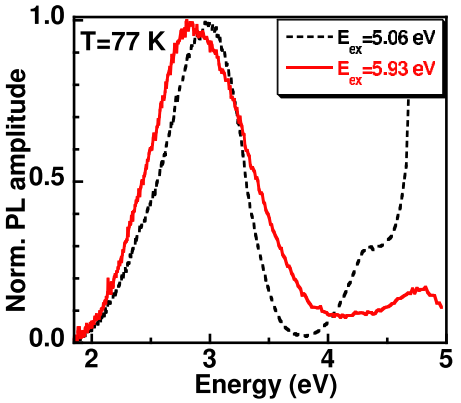

FIG. 5. (Color online) Normalized PL emission spectra of $SrHfO_3$ at 77 K. Excitation energies are reported in the legend.

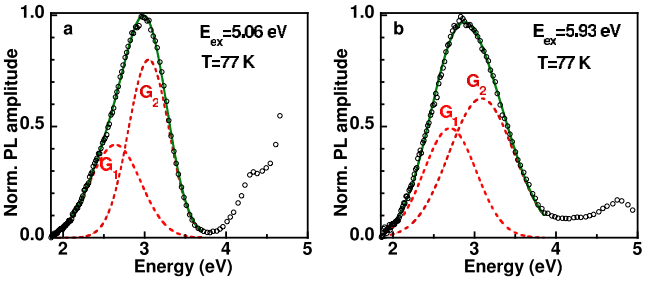

FIG. 6. (Color online) Gaussian decomposition of PL emission spectra displayed in Fig. 5. Empty circles are experimental data, solid line is the fit to the data, and dashed lines are Gaussian components G_1 and G_2.

that this reduction is accompanied by decreasing emission intensity of the G_1 band. In particular, at the emission energy 3.6 eV, with almost no contribution of the G_1 band [cf. Figs. 6(a) and 6(b)], the contribution of the 5.0 eV excitation band is fairly weak (Fig. 4). This observation leads to the conclusion that the G_2 emission band is excited exclusively in the exciton absorption peak and therefore is of excitonic origin (as expected based on comparison with similar materials reported above). Due to the significant Stokes shift the emission is most probably associated with an exciton trapped around a lattice defect and designated TE_{II}. On the other hand the excitation spectrum of the G_1 band at 2.2 eV (where no contribution of the G_2 band is expected) in Fig. 7 features a broad band that corresponds to a mixture of 5.0 eV and exciton absorption bands. The G_1 band is most probably associated with the emission of a lattice defect, DE_I. The defect is excited either directly via its 5.0 eV excitation band or indirectly via the exciton absorption due to the overlap between the 5.0 eV excitation band and the 5.1 eV STE emission discussed above. It would be interesting to assess whether TE_{II} is trapped around the same defect responsible for the DE_I RL emission or whether there are two different lattice defects in play giving rise to two emissions in similar spectral regions. However, based on current data such an assessment cannot be made.

The 4.0 eV band is not contributing significantly to the total RL intensity. Its excitation spectrum at 77 K in Fig. 4 features a band at about 5.2 eV which is probably associated with another impurity or lattice defect, DE_{II}.

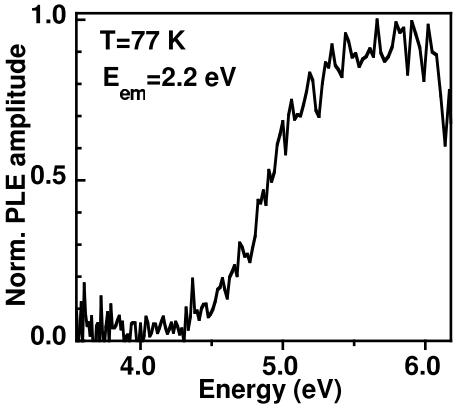

FIG. 7. Normalized PL excitation spectra of $SrHfO_3$ at 77 K and 2.2 eV.

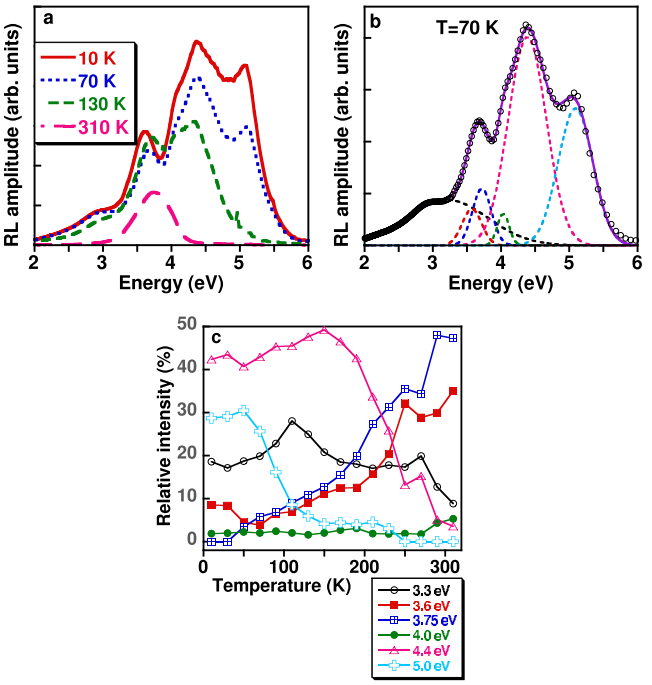

FIG. 8. (Color online) (a) X-ray excited RL spectra of $SrHfO_3:Pb^{2+}$ at selected temperatures. (b) Example of the Gaussian decomposition of the RL spectrum at 70 K. Empty circles are experimental data, solid line is the fit to the data, and dashed lines are Gaussian components. (c) Temperature evolution of relative intensity of each peak with respect to the total emission intensity. The spectral positions are indicated in the legend.

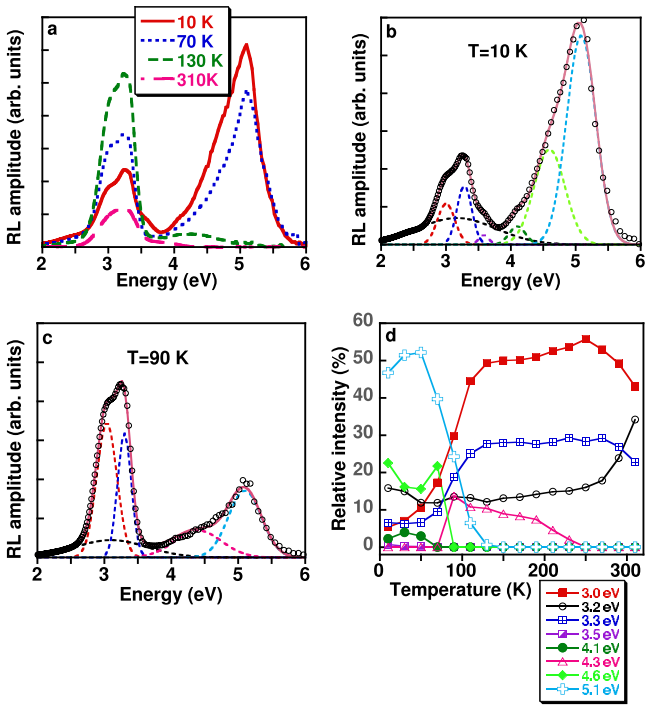

FIG. 9. (Color online) (a) X-ray excited RL spectra of $SrHfO_3:Ce^{3+}$ at selected temperatures. (b) Example of the Gaussian decomposition of the RL spectrum at 10 K. Empty circles are experimental data, solid line is the fit of the sum of seven Gaussians to the data, and dashed lines are Gaussian components. (c) Example of the Gaussian decomposition at 90 K. Empty circles are experimental data, solid line is the fit of the sum of five Gaussians to the data, and dashed lines are Gaussian components. (d) The temperature evolution of relative intensity of each peak with respect to the total emission intensity. The spectral positions are indicated in the legend.

To summarize, we tentatively assign the emission bands observed in undoped $SrHfO_3$ in the following way: the 5.1 eV band is the emission of STE, the 4.6 eV is an emission due to an exciton trapped around an impurity or lattice defect, TE_I, (with possible contribution of a defect), the 3.0 eV band is composed of TE_{II} and DE_I components and the 4.0 eV band is the emission of another unspecified impurity or defect (DE_{II}).

B. $SrHfO_3$ activated by Pb^{2+} or Ce^{3+}

In Fig. 8(a) we present x-ray excited RL spectra of $SrHfO_3:Pb^{2+}$ with the 0.03 mol % dopant concentration at selected temperatures. The spectra were measured in the 10–310 K temperature interval. The Gaussian decomposition of all spectra shows the presence of 6 bands at 3.3, 3.6, 3.75, 4.0, 4.4, and 5.1 eV as demonstrates an example in Fig. 8(b) reporting the decomposition at 70 K, where all Gaussian bands are present. At the lowest temperatures one of the two emission bands associated with the Pb^{2+} activator is missing, as already reported in Ref. 11 (the parameters of all Gaussians are listed in Table I). The temperature evolution of the relative intensity of each peak with respect to the total emission intensity is shown in Fig. 8(c).

The comparison with the undoped sample shows that the STE band at around 5 eV is present while that at 4.6 eV is missing or masked by a new intense 4.4 eV band. The weak 4.0 eV defect band DE_{II} is also present. The $TE_{II}+DE_I$ band centered at 3 eV in the undoped sample seems to be shifted to higher energy, 3.3 eV. This might be due to its composed character or by a perturbation of either TE_{II} or DE_I, or both, by the presence of the activator. Then there are three new bands appearing in the Pb^{2+}-doped sample with respect to the undoped sample. Two bands at 3.6 and 3.75 eV were associated with the presence of Pb^{2+} ion.[11] This association is evident also from RL spectra of samples with a higher concentration of lead shown later. Figure 8(c) demonstrates the competition of all recombination centers for carrier capture. Around RT the emission process is completely dominated by recombination at Pb^{2+} centers. The $TE_{II}+DE_I$ band at 3.3 eV shows a similar behavior as in the undoped sample until above 100 K. Then the temperature evolution of its relative intensity is affected by competition with the Pb center. However, unlike in the undoped sample, the band does not dominate the emission at low temperatures. There is a new low T dominant band at 4.4 eV. Its similar, however different energy, as well as the temperature evolution similar to the TE_I band at 4.6 eV in the undoped sample brings the idea of its association with the Pb-perturbed TE (TE_{Pb}). At higher temperatures it is probably also suppressed by competition with the Pb^{2+} emission center.

In Fig. 9(a) we present x-ray excited RL spectra of

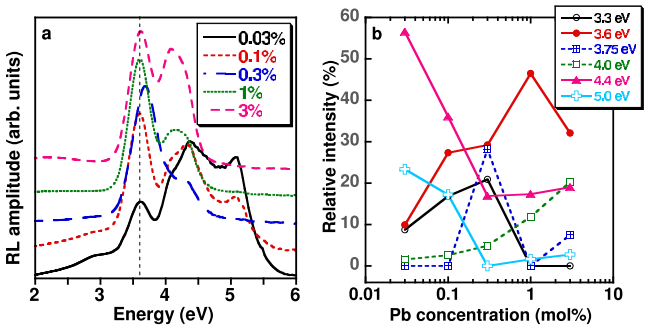

FIG. 10. (Color online) (a) RL spectra corresponding to various Pb^{2+} concentrations at 10 K. (b) Relative intensities of associated Gaussian bands (with respect to the total intensity).

$SrHfO_3:Ce^{3+}$ with dopant concentration of 0.1 mol % at selected temperatures. The spectra were measured in the 10–310 K temperature interval. The Gaussian decomposition of all spectra shows the presence of seven bands at 3.0 eV, 3.2 eV, 3.3 eV, 3.5 eV, 4.1 eV, 4.3 eV, 4.6 eV and 5.1 eV as demonstrate examples at 10 K and 90 K displayed in Figs. 8(b) and 8(c), respectively (the parameters of all Gaussians are listed in Table I). The temperature evolution of the relative intensity of each peak with respect to the total emission intensity is shown in Fig. 9(d).

Again the comparison with the undoped sample shows that the STE band at 5.1 eV is present as well as the weak 4.0 eV DE_{II} defect band. The $TE_{II}+DE_I$ band is centered at 3.2 eV, again somewhat shifted with respect to the undoped sample possibly for the same reasons as in the case of Pb^{2+} activator. We also individuated a weak band at 3.5 eV that might be due to a Pb^{2+} contamination of the sample. We observe the Ce^{3+} band with its characteristic doublet structure peaking at 3.0 and 3.3 eV. The remaining 4.3 and 4.6 eV bands are interchanging their presence. At low T there is only the 4.6 eV band resembling that found in the undoped sample. From 90 K on, there is only the 4.3 eV band, resembling that found in the Pb-doped sample, which in this case could be analogously assigned to the Ce-perturbed TE_{Ce}. That would indicate that for low temperatures the exciton is more likely trapped around a lattice defect as in the undoped sample while from 90 K it is more likely trapped at the defect perturbed by the presence of Ce.

C. Concentration dependence of $SrHfO_3:Pb^{2+}$ radioluminescence

The RL spectra of $SrHfO_3:Pb$ with various concentrations of Pb^{2+} were measured in the 10–310 K temperature interval. For an intermediate activator concentration, 0.3%, we studied the samples prepared by two different methods, namely acetate-citrate combustion and solid-state reaction. Figure 10(a) shows the spectra corresponding to various Pb^{2+} concentrations at 10 K. We performed the Gaussian decomposition of these spectra and the relative intensities of the bands (with respect to the total intensity) are displayed in Fig. 10(b). The figure demonstrates that with increasing concentration (up to the optimal value of 0.3 mol %) the activator centers become more effective in trapping free carriers at the expense of other recombination centers in the host lattice. At higher concentrations the effectiveness of the activator centers gets reduced. The highest RL output associated with the Pb^{2+} center (3.6 and 3.75 eV bands) is obtained for an intermediate concentration, 0.3 mol %.

There is an additional interesting feature to be noticed in Figs. 10(a) and 10(b). As pointed out in Ref. 11 (and also evident from the results of Gaussian decomposition in this work) the emission associated with the Pb^{2+} center consists of two closely lying bands manifesting a thermally induced change of the relative populations of their corresponding excited states. At the lowest temperatures the low energy band (3.6 eV) dominates the Pb emission. Figure 10(b) confirms this statement for all concentrations except that of 0.3% (sample prepared by A-C combustion method). At this concentration both bands (3.6 and 3.75 eV) similarly contribute to the activator emission [see Fig. 10(b)] which is also manifested as the high temperature shift of the emission maximum with respect to that of other concentrations [cf. Fig. 10(a)]. Evidently, for reasons unknown, in this sample two different Pb centers feature similar efficiency in trapping the free carriers from low to intermediate temperatures. By contrast, in all other samples the low-temperature region is absolutely dominated by the low-energy 3.6 eV band. The same is true as well for the sample with 0.3% Pb^{2+} concentration prepared by the solid state reaction method (not shown).

IV. CONCLUSION

In this work we study in detail the x-ray excited RL emissions together with related PL excitation and emission spectra in $SrHfO_3$-based scintillators to better understand the underlying scintillation mechanism. The Gaussian decomposition of undoped $SrHfO_3$ RL spectra manifests the presence of four emission bands. Based on their temperature behavior, excitation spectra, and comparison with similar materials reported in the literature we tentatively assign the observed bands in the following way. The highest energy bands peaking at 5.1 eV and 4.6 eV are associated with emissions of self-trapped exciton and exciton trapped around impurity or lattice defect (with possible contribution of a defect), respectively. The temperature dependence of the intensities of these bands indicates the onset of thermal disintegration of the exciton at about 70–90 K. The minor band at about 4 eV is associated with some impurity or lattice defect. The most intense low-energy band at about 3 eV turns out to be composed of two components that are of excitonic (most probably trapped exciton) and defect-related character. When doped by Ce^{3+} or Pb^{2+} luminescence activators, two and three new emissions appear, respectively. They are either due to the activators themselves or due to excitonic states perturbed by their presence. The temperature dependence of all RL spectra demonstrates a competition between activators and intrinsic or defect centers in the carrier capture. Around room temperature the emission process is completely dominated by recombination at activator centers.

ACKNOWLEDGMENTS

The financial support of the Italian CARIPLO Foundation project "Energy transfer and trapping phenomena in nanostructured scintillator materials," 2008–2011, the Czech under Grant No. GAAV KAN300100802 and the DESY under Grant No. I-20090104 EC project are gratefully acknowledged.

[1] C. Rossel, M. Sousa, C. Marchiori, J. Fompeyrine, D. Webb, D. Caimi, B. Mereu, A. Ispas, J. P. Locquet, H. Siegwart, R. Germann, A. Taponnier, and K. Babich, Microelectron. Eng. **84**, 1869 (2007).

[2] A. Feteira, D. C. Sinclair, K. Z. Rajab, and M. T. Lanagan, J. Am. Ceram. Soc. **91**, 893 (2008).

[3] S. Yamanaka, T. Maekawa, H. Muta, T. Matsuda, S. Kobayashi, and K. Kurosaki, J. Alloys Compd. **381**, 295 (2004).

[4] H. Yamamoto, M. Mikami, Y. Shimomura, and Y. Oguri, J. Lumin. **87-89**, 1079 (2000).

[5] S. L. Dole and V. Venkataramani, U. S. Patent No. 5124072 (1992).

[6] E. V. van Loef, W. M. Higgins, J. Glodo, Ch. Brecher, A. Lempicki, V. Venkataramani, W. W. Moses, S. E. Derenzo, and K. S. Shah, IEEE Trans. Nucl. Sci. **54**, 741 (2007).

[7] Y. M. Ji, D. Y. Jiang, L. S. Qin, J. J. Chen, T. Feng, Y. K. Liao, Y. P. Xu, and J. L. Shi, J. Cryst. Growth **280**, 93 (2005).

[8] H. Retot, A. Bessiere, A. Kahn-Harari, and B. Viana, Opt. Mater. **30**, 1109 (2008).

[9] M. Villanueva-Ibanez, C. Le Luyer, S. Parola, O. Marty, and J. Mugnier, J. Sol-Gel Sci. Technol. **31**, 277 (2004).

[10] M. Villanueva-Ibanez, C. Le Luyer, S. Parola, C. Dujardin, and J. Mugnier, Opt. Mater. **27**, 1541 (2005).

[11] E. Mihóková, F. Moretti, N. Chiodini, A. Lauria, M. Fasoli, A. Vedda, A. Nale, M. Nikl, and P. Boháček, IEEE Trans. Nucl. Sci. **57**, 1250 (2010).

[12] V. Jarý, M. Nikl, E. Mihóková, P. Boháček, B. Trunda, K. Polák, V. Studnička, and V. Múčka, Radiat. Meas. **45**, 406 (2010).

[13] A. Lauria, N. Chiodini, E. Mihóková, F. Moretti, A. Nale, M. Nikl, and A. Vedda, Opt. Mater. **32**, 1356 (2010).

[14] V. Jarý, E. Mihóková, M. Nikl, P. Boháček, A. Lauria, and A. Vedda, Opt. Mater. (to be published).

[15] The full exciton absorption/excitation peak could not be measured due to limits of apparatus used in this particular measurement.

[16] V. M. Longo, L. S. Cavalcante, M. G. S. Costa, M. L. Moreira, A. T. de Figueiredo, J. Andres, J. A. Varela, and E. Longo, Theor. Chem. Acc. **124**, 385 (2009).

[17] R. Leonelli and J. L. Brebner, Phys. Rev. B **33**, 8649 (1986).

[18] J. F. Meng, Y. B. Huang, W. F. Zhang, Z. L. Du, Z. Q. Zhu, and G. T. Zou, Phys. Lett. A **205**, 72 (1995).

[19] R. I. Eglitis, E. A. Kotomin, V. A. Trepakov, S. E. Kapphan, and G. Borstel, J. Phys.: Condens. Matter **14**, L647 (2002).

[20] Y. S. Lee, J. S. Lee, T. W. Noh, D. Y. Byun, K. S. Yoo, K. Yamaura, and E. Takayama-Muromachi, Phys. Rev. B **67**, 113101 (2003).

[21] V. S. Vikhnin, A. A. Kaplyanskii, A. B. Kutsenko, G. K. Liu, J. V. Beitz, and S. E. Kapphan, J. Lumin. **94-95**, 775 (2001).

[22] V. S. Vikhnin, R. I. Eglitis, S. E. Kapphan, E. A. Kotomin, and G. Borstel, Europhys. Lett. **56**, 702 (2001).

[23] V. S. Vikhnin, R. I. Eglitis, S. E. Kapphan, G. Borstel, and E. A. Kotomin, Phys. Rev. B **65**, 104304 (2002).

[24] The full width at half maximum (FWHM) of G_1 is 0.75 ± 0.05. The somewhat larger FWHM of G_2 in Fig. 6(b) (0.9 eV) with respect to Fig. 6(a) (0.6 eV) can be due to some perturbation of the emitting center that changes with the excitation energy.